# Decision-Level Fusion Performance Improvement From Enhanced HRR Radar Clutter Suppression

**BART KAHLER**
**ERIK BLASCH**

**Airborne radar tracking in moving ground vehicle scenarios is impacted by sensor, target, and environmental dynamics. Moving targets can be characterized by 1-D High Range Resolution (HRR) Radar profiles with sufficient Signal-to-Noise Ratio (SNR). The amplitude feature information for each range bin of the HRR profile is used to discern one target from another to help maintain track or to identify a vehicle. Typical radar clutter suppression algorithms developed for processing moving ground target data not only remove the surrounding clutter, but a portion of the target signature. Enhanced clutter suppression can be achieved using a Multi-channel Signal Subspace (MSS) algorithm, which preserves target features. In this paper, we (1) exploit extra feature information from enhanced clutter suppression for Automatic Target Recognition (ATR), (2) present a Decision-Level Fusion (DLF) gain comparison using Displaced Phase Center Antenna (DPCA) and MSS clutter suppressed HRR data; and (3) develop a confusion-matrix identity fusion result for Simultaneous Tracking and Identification (STID). The results show that more channels for MSS increase identification over DPCA, result in a slightly noisier clutter suppressed image, and preserve more target features after clutter cancellation. The paper contributions include extending a two-channel MSS clutter cancellation technique to three channels, verifying the MSS is superior to the DPCA technique for target identification, and a comparison of these techniques in a novel multi-look confusion matrix decision-level fusion process.**

Manuscript received April 16, 2009, Nov. 24, 2009, April 22, 2010, April 28, 2011; released for publication May 10, 2011.

Refereeing of this contribution was handled by Dr. Robert Lynch.

Authors' addresses: B. Kahler, SAIC, Dayton, OH; E. Blasch, AFRL, Dayton, OH.



## 1. INTRODUCTION

Many surveillance systems incorporate High Range Resolution (HRR) radar and Synthetic Aperture Radar (SAR) modes to be able to capture moving and stationary targets. Feature-, signature-, and categorical-aided tracking and Automatic Target Recognition (ATR) applications benefit from HRR radar processing. Successful Simultaneous Tracking and Identification (STID) [6, 12, 65] applications exploit feature information to determine the target type and dynamics. Throughout the paper, we use identification, as opposed to recognition, to clarify the process of distinguishing between two targets of the same classification label or allegiance type.

To maximize a search area, airborne systems operate at standoff ranges to detect targets and initiate tracks [3, 5]. After target acquisition and track initiation, tracking systems then transition into a track maintenance mode. However, closely spaced targets require feature analysis to identify the targets. In track maintenance, HRR radar affords dynamic processing analysis for vehicle tracking and signal feature extraction (range, angle, aspect, and peak amplitudes) for target detection and identification [7].

Pattern recognition algorithms applied to ATR problems are typically trained on a group of desired objects in a library to gain a statistical representation of each objects' features. One-dimensional (1-D) HRR classifiers exploit the location and peak amplitude information contained in the HRR signatures [19, 38]. HRR classifiers align input signatures to the library templates or models [16] and determine the best correlation value for the aligned features. HRR ATR algorithms often apply a threshold to the best score to reject questionable objects before making identification or class label decisions. As per the previous work on target identification from HRR signatures, we improve existing capabilities by increasing the peak amplitudes and refine range-bin locations through clutter suppression techniques.

A number of papers have been published that evaluate one-dimensional (1-D) HRR ATR solutions [22, 27, 46, 62, 63]. Classifiers have been developed for correlation [34], Bayes and Dempster Shafer information fusion [11], entropy and information theory analysis [8], and neuro-fuzzy methods [10]. The classifier results have been used for tracking [9, 66] and multi-look HRR identification [53, 67]. Other approaches include eigenvalue template matching [51], Eigen-Extended Maximum Average Correlation (EEMACH) filters [31] and likelihood methods accounting for Rician, amplitude, specular, and diffuse, Cisoid scattering [18]. Since we utilize a combination of sensor and exploitation algorithms (with reported decisions) we are not afforded feature or signal-level fusion options. Using inspiration from the above ATR fusion methods, we incorporate maximum-likelihood Bayesian methods into our novel Confusion Matrix Decision-Level Fusion (CM-DLF) algorithm.

Although the ATR process seems straightforward, misidentification or rejection of an input object as a viable target occurs because of feature extraction differences over different operating conditions. Extended operating conditions (EOCs) such as the target being obscured from the sensor, targets adjacent to another object, and target transitions from moving to stationary and back to a moving state in a traffic scenario unexpectedly alter the features. The importance and impact of EOCs is critical to ATR performance [25]. The quality of the information used in joint tracking, classification, and identification [1, 32, 36, 64] can be determined through Bayes, Dempster-Shafer, or Dezert-Smarandache Theory (DSmT) analysis methods [60]. The clutter-suppressed CM-DLF approach enhances both EOC target identification through minimizing residual range and Doppler noise and enhancing track accuracy through pose angle determination with the correct target shape (features in range-Doppler space).

HRR ATR algorithm performance is impacted by the quality of the features available in the 1-D HRR profiles. Missing target features in training data will alter the library templates formed resulting in poorer identification performance. The presence of EOCs will degrade 1-D test signatures and the corresponding classifier performance. Since the signature data used by ATR algorithms is not always pristine, information fusion methods have been developed such as multi-look ATR, decision level fusion (DLF), and feature level fusion (FLF) in an effort to enhance identification performance from HRR radar data. Improved HRR processing prior to 1-D HRR profile formation (i.e., clutter cancellation) should improve the target features available or reveal more target features, resulting in higher quality 1-D signatures and improved ATR performance.

For many decades, researchers have been developing methods for target identification (ID) through HRR analysis either focused on the radar data itself (e.g., clutter suppression) or the target classification (e.g., pattern recognition methods), which lack the ability to deal with high-density closely-spaced moving target IDs. As simultaneous tracking and identification methods are being applied to urban areas, targets are closer together, have maneuvering dynamics, and are of similar shape. To compensate for these needs, we have coordinated the development of (1) MSS clutter suppression enhancements to deal with closely spaced targets, (2) designed a novel confusion-matrix decision-level fusion approach to take sensor-exploitation likelihood results and update target ID tracks, and (3) combined clutter suppression and CM-DLF for enhanced target signature analysis through movements. Conceptually, target identification improves from having more (a) salient features, (b) spatially and temporally refined features in range-Doppler space, and (c) recursively fused features from different perspectives.

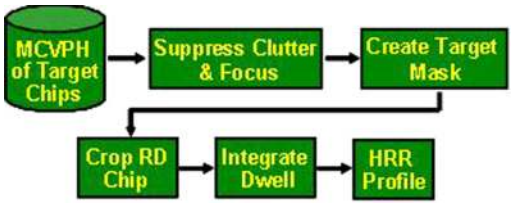


Fig. 1. 1-D HRR profile formation process.

This paper reviews HRR data processing in Section 2, discusses the implementation of a standard two-channel DPCA clutter cancellation method, presents an improved multi-channel signal subspace (MSS) clutter suppression algorithm, and compares the resulting clutter-canceled target chips and target-to-clutter ratios. In Section 3, a multi-look decision level fusion identification method is presented along with performance metrics. Section 4 presents the DPCA and MSS 1-D HRR identification performance in both single-look and multi-look scenarios and Section 5 discusses conclusions and future work.

## 2. HRR DATA PROCESSING

Focused 1-D HRR radar profiles of *moving targets* may be generated with enhanced target-to-clutter ratios. The moving target is first chipped from the motion-compensated video phase history (MCVPH) radar data for each channel available. The chipped target of the trailing channel is aligned to the target chip of the lead channel for clutter suppression and focusing, as illustrated in Fig. 1. The processing results in a two-dimensional range-Doppler (RD) chip (shown in Fig. 5) that is masked using binary morphology to determine the mean clutter level, target length, and target edges in the chip. The range-Doppler chip is then cropped about the Doppler extent of the target mask before computing the mean of all sub-aperture images. The integration over the dwell time is conducted, which is the duration that the target remains in the radar's beam during each scan. The maximum scatters from each range bin are kept to form the 1-D HRR profile.

*Stationary targets* from SAR imagery may also be formed into 1-D HRR profiles using a similar process. For targets in SAR imagery, constant-false alarm rate (CFAR) detection is performed first, followed by target mask formation using binary morphology. The formation process crops around the target mask and computes the mean of all sub-aperture images, keeping the maximum scatters from each range bin to form the stationary HRR profile. Shown in Fig. 1 is the general profile formation process flow.

Recent research [19] has shown that HRR profiles formed from SAR imagery of stationary targets have comparable features to profiles of the same target moving at corresponding collection geometries as shown in Fig. 2. The amplitude of the moving target range profile (dashed red line) is lower relative to the stationary target profile (solid blue line) because some of the moving

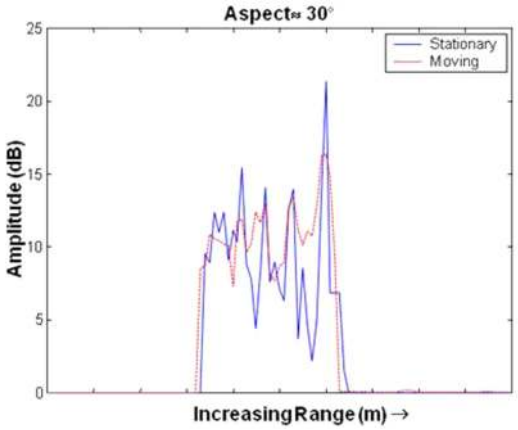


Fig. 2. Comparison of moving/stationary 1-D HRR profiles.

target energy is lost during clutter cancellation while forming the HRR profile. HRR profiles formed from SAR images do not require clutter cancellation in the range profile formation process. However, the strongest scattering features of the target still correlate in range between the moving and stationary target HRR profiles. Since HRR profiles can be formed directly from moving platform HRR collections or extracted from SAR target chips, we are able to utilize collected SAR images for HRR testing and analysis.

### 2.1. General Clutter Suppression

Clutter suppression of airborne radar data for moving ground targets is a crucial step in target detection and identification. Clutter suppression is needed to enhance the target signature while reducing the competing ground clutter energy surrounding the moving target [13]. As shown in the results in Section 2.4, three visible improvements in Figs. 8–10 that compare two-channel versus three-channel MSS are: (1) better estimate of energy return to range resulting in the estimate of the target length, (2) reduced Doppler clutter to enhance target movement estimates for tracking, and finally, (3) more salient features from which to do a target identification from either template or model matching.

Typically, clutter suppression techniques have the unintentional side effect of reducing some of the target energy while suppressing the ground clutter. Although the target-to-clutter ratio may improve greatly, a reduction in the target features is inevitable, which impacts target tracking and identification performance. The processing of airborne multi-channel radar data to cancel the clutter near moving ground targets can be accomplished through a variety of techniques such as Doppler filtering, space-time adaptive processing (STAP), or displaced phase center antenna (DPCA) processing [13].

*Doppler filtering* is a technique used with adaptive radars that sense the Doppler distribution of clutter and adjust the radar parameters in an attempt to maximize the signal to clutter ratio. Clutter suppression is accomplished by obtaining a separate coherent output from each channel of an antenna array and applying a unique

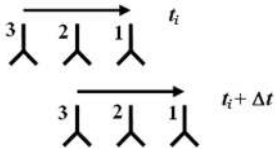


Fig. 3. Three-channel antenna configuration.

complex weight to each channel. Then the weighted channels are added coherently to cancel the clutter energy [13, 21, 33].

A two-dimensional filtering technique known as *Space Time Adaptive Processing* (*STAP*) [21, 28, 29, 49] uses the Doppler frequency, sensor platform velocity, and direction of arrival information to achieve clutter cancellation. Adaptive filter weights are determined for the temporal and spatial domains after sampling a coherent train of pulses. These weights then form a two-dimensional space-time clutter filter that can be applied to the data to eliminate ground clutter. STAP processing is robust to errors and can simultaneously suppress clutter returns and jamming signals [17, 40, 48].

In *DPCA* processing, radar motion compensation reduces the Doppler spread of ground clutter induced by the sensor platform [30, 35, 41]. A multi-channel airborne radar configuration often has a pair of antennas positioned so that as the platform travels in time, the position of the trailing antenna will occupy approximately the same position of the lead antenna at some delta time. Essentially, for a given time interval, one antenna position is fixed. Clutter suppression is accomplished by subtracting the received signal from the trailing antenna at the delta time from the received signal of the lead antenna at the initial time of the processing interval [37, 39, 58].

Both STAP and DPCA are capable of cancelling main beam and side lobe clutter for multi-channel airborne radars with two or more antenna phase centers [40]. In this paper, an available DPCA two-channel algorithm was chosen for comparison to the multi-channel signal subspace algorithm.

A three-channel antenna configuration is shown in Fig. 3, where antenna number 1 is the lead channel for the collected data. The concept of DPCA processing is illustrated in Fig. 3 for a three-channel antenna array configuration. The positions of the antennas are shown at the initial time, $t_i$, and with platform motion at some time interval, $t_i + \Delta t$, where $\Delta t$ is the change in time. Through DPCA processing, two antenna positions will appear to be at the same physical location for the array depicted in Fig. 3. Therefore, clutter cancellation is possible where channel 2 at $t_i$ and channel 3 at $t_i + \Delta t$ line up and where channel 1 at $t_i$ and channel 2 at $t_i + \Delta t$ are aligned.

The radar data processed for this paper was collected at X-Band with the aircraft traveling in a linear flight path north of the scene center collecting in spotlight mode at a depression angle of 8.97 degrees and at a weighted resolution of approximately 12 inches. As

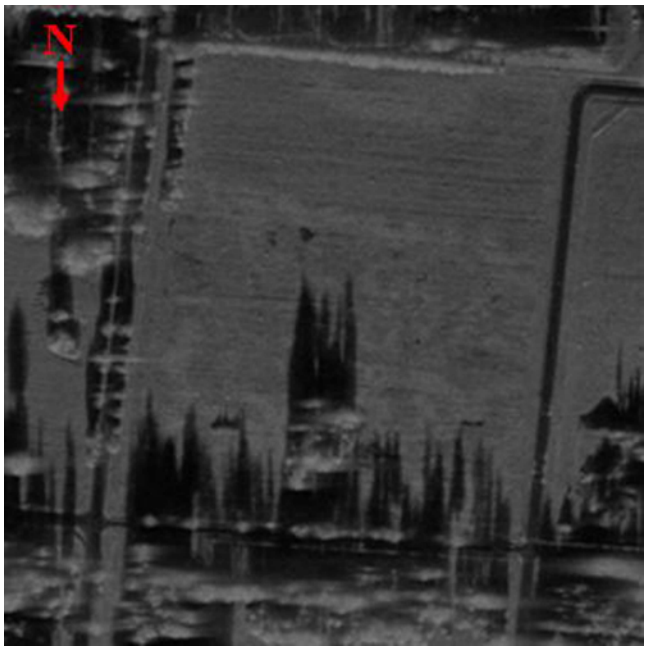


Fig. 4. SAR image of collection site.

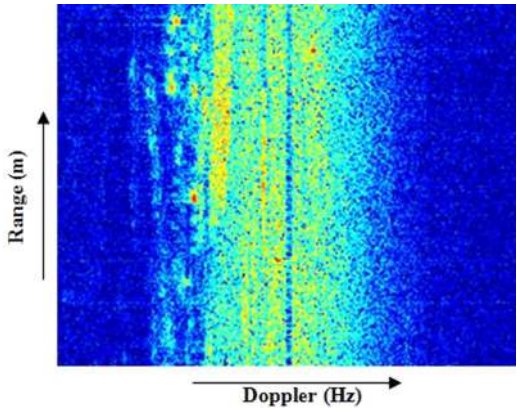


Fig. 5. Example of target chip before clutter suppression.

illustrated in the SAR image of Fig. 4, the center of the collection site was a rectangular grassy area with roads along the western, eastern, and southern borders of the target area. Wooded areas surround the grassy rectangle along the northern, eastern, and southern portions of the scene. In the scenario, civilian vehicles (i.e., trucks and cars) are traveling along the roads in all directions.

The image chips used in the processing discussion are of the test vehicle moving south along the western road. In Fig. 5, an example range-Doppler chip of the target vehicle from channel 1, the lead channel, before clutter suppression is shown. The y-axis is a function of the range bins, which when multiplied by the pixel spacing, is measured in meters (m). The x-axis is in Hz, where the maximum Doppler shift for the clutter is determined as (2∗velocity of the sensor)/wavelength.

The two-channel DPCA processing approach is explained in Section 2.2. Section 2.3 explains the multichannel signal subspace algorithm and the clutter suppression results of the target chip are presented in Section 2.4.

### 2.2. DPCA Technique

In Section 2.1, the DPCA processing was introduced. The DPCA algorithm used in this work was developed for measured data from a radar array of two antennas oriented along the sensor platform path of travel. In general, the data from the trailing antenna (channel 2 of Fig. 6) is aligned to the lead channel (channel 1 of Fig. 6), where the phases are adjusted so that the aligned channels appear to be at the same location in space, and finally, the channels are subtracted to suppress the stationary clutter. Fig. 6 illustrates the processing steps and data flow of the DPCA technique.

The DPCA algorithm is provided motion-compensated phase history data for both the lead (channel 1) and trailing (channel 2) channels. Channel 2, the trailing channel data, contains extra pulses to address minor offset delays between the channels. *Alignment* of the range and pulse offset is conducted to roughly get channel 2 to approximate channel 1. Then, the antenna patterns are estimated for each channel and an antenna *pattern correction* is applied to channel 2 so that the channels are similar. A *phase correction* is determined in the Doppler compressed domain to account for differences in the frequency direction not already corrected by coarse channel alignment and to address small phase variations between the channels caused by any minor hardware differences in the collection system. The phase correction factor is applied to the data of channel 2. Further *phase adjustments* are determined in the range-Doppler domain and applied to channel 2 to account for any shift in the fast-time samples. A series of additional phase corrections are applied to channel 2 by the DPCA algorithm to improve the *fine alignment* of channel 2 to channel 1 to maximize the target-to-clutter ratio. These

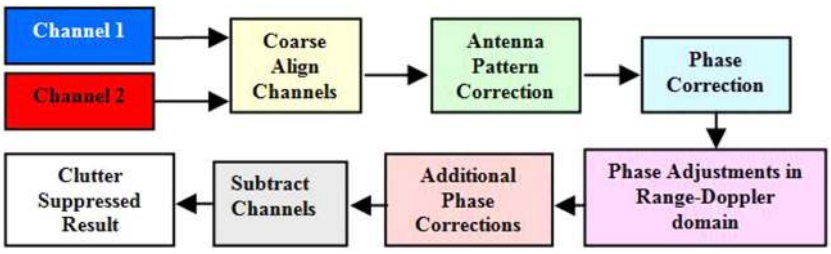


Fig. 6. Two-channel DPCA process flow.

additional corrections require that any target-like objects in the data be avoided so that the target energy is not included in phase correction estimates as was done in the determination of the previous correction factors. The correction factors account for time varying phase differences between both channels being applied to channel 2. Next, a fast-time magnitude and phase correction is applied in the Doppler compressed domain to the data of channel 2. Then a *smoothing technique* is applied to the data resulting in a trailing channel that has been equalized to the lead channel. This completes the alignment process of channel 2 to channel 1. Now that channel 2 appears to be the same as channel 1, the *subtraction* of the channels result in the *cancellation of stationary clutter* in the scene. The baseline clutter suppressed data is represented by $f_d(k,n) = f_1(k,n) - f_2(k,n)$, where $f_1$ is channel 1, $f_2$ is the equalized phase history data of channel 2 to that of channel 1, $k$ is the fast-time index, $n$ is the pulse number, and $f_d$ is the clutter-cancelled result.

The DPCA adaptive clutter cancellation method presented will be applied to the data used in this work to ultimately produce the DPCA 1-D HRR profiles. In an effort to improve the 1-D HRR profiles and preserve more target features, a multi-channel signal subspace technique is developed in Section 2.3.

## 2.3. Multi-channel Signal Subspace Technique

The exploitation of the additional information of a third channel in the phased array radar yields more precise clutter estimation and results in better suppression of unwanted clutter returns. By using the information of all three channels, more target features are preserved in the clutter canceled image [26]. Increasing available target features should translate into better target identification performance. This section will briefly explain the background, the theory behind two channel clutter suppression, and extend this technique to three-channel clutter cancellation.

### 2.3.1. Signal Subspace Background

The *Multi-channel Signal Subspace* (MSS) technique is based on 2-D adaptive filtering principles. The process has been applied to a wide variety of data processing problems in the literature [54] such as SAR change detection, [47] image fusion of radar surveillance data, [56, 57] medical imaging, and video processing [20, 54]. Most of the work with signal subspace processing has focused on data pairs either separated spatially (e.g., two channel phased array radar data) or separated temporally (e.g., such as electro-optical images collected at different times) as discussed in the literature by Soumekh and others [54, 55, 57].

The development of a true multi-channel, greater than two, signal subspace algorithm for use with a multi-channel radar system consisting of a planar antenna array of 22 receiver channels seemed likely [2]. However, the received power at each channel was too weak to form an image of sufficient quality for further processing. This issue was resolved by splitting the data from the 22 channels into a pair of 11 receiver channel groups that were summed to improve the signal to noise level [57]. Once the planar antenna array is represented by two receive channels, the signal subspace processing technique is applied to clutter-cancel the data. In the next section, the process for two-channel clutter suppression will be explained.

### 2.3.2. Dual-Channel Signal Subspace Technique

The dual-channel radar system discussed in this section will have a pair of antennas in a phased array similar to what is illustrated in Fig. 3, but without the third channel being present. Channel 1 will be the lead channel and channel 2 will be the trailing channel. In keeping with the convention found in the literature, let $f_1(x,y)$ represent the range-Doppler image formed from the motion-compensated data from channel 1 over a coherent processing interval (CPI) of 128 ms. Then, $f_2(x,y)$ will be the range-Doppler image formed from the motion-compensated data from channel 2 after a slow-time alignment with channel 1. Since the channel 2 range-Doppler image is a linear combination of channel 1 and any shifted versions, $f_2(x,y)$ can then be modeled by [54, 20], $f_2(x,y) = f_1(x,y) \otimes h(x,y) + f_e(x,y)$; where $\otimes$ is the convolution operator, $f_e(x,y)$ represents the target motion in the range-Doppler image, and $h(x,y)$ is the impulse response representing the relative shift in each range-Doppler image due to differences in the two receive channels of the sensor system.

Gain and phase ambiguities caused by known and unknown factors, such as differences between the antenna patterns or antenna vibration, in the two receive channels may dominate the moving target signature in the imagery. These differences are treated as an error signal in the collected data. The DPCA approach reduces the error signal to a set of pre-determined functions that are estimated and accounted for deterministically. The MSS technique applied to a dual antenna sensor system views the error estimation process as completely stochastic.

Signal subspace theory estimates $h(x,y)$ from $f_1(x,y)$ and $f_2(x,y)$ resulting in the error function, $\hat{h}(x,y)$ [54, 56]. This is accomplished by minimizing the squared error between $f_2(x,y)$ and its estimated version given by

$$\hat{f}_2(x,y) = \hat{h}(x,y) \otimes f_1(x,y) \tag{1}$$

where $\hat{f}_2(x,y)$ is determined by projecting $f_2(x,y)$ on to a set of orthogonal basis functions defined by $f_1(x,y)$ [54]. The orthogonal basis functions can be computed using any one of accepted decomposition/orthogonalization techniques such as singular value decomposition, QR orthogonalization, or the Gram-Schmidt procedure. QR orthogonalization was used in the MSS implementation that generated the results of this paper where in practice $\hat{h}(x,y) \otimes f_1(x,y)$ is estimated instead

of $\hat{h}(x,y)$. In general, the spatially-invariant difference over the entire image is represented by [20, 54],

$$\hat{f}_d(x,y) = f_2(x,y) - \hat{f}_2(x,y). \quad (2)$$

To suppress unwanted clutter in radar data, the error function is estimated with overlapping odd-sized blocks over the entire image to account for the spatially varying nature of the phase in the imagery. The entire range-Doppler image is divided into rectangular blocks containing an odd number of pixels and processed to estimate the error function. The blocks of image pixels were moved so that some portion of the rectangular patch overlapped a previously processed block until the entire subdivided image had been processed. This results in a clutter-cancelled image given by [56],

$$\hat{f}_d(x_i,y_i) = \sum_{l=1}^{L} [f_2(x_i,y_i) - \hat{f}_2(x_i,y_i)] I_l(x_i,y_i) \quad (3)$$

for a two channel phased array radar system. $L$ is the number of overlapping blocks processed, $i$ is the odd number of pixels per block, and $I_l$ is an identity matrix. The MSS implementation in this paper used square patches in the processing represented by $(x_i,y_i)$, but in general a rectangular block represented by $(x_i,y_j)$ could be used for an $i$-by-$j$-dimensional block. The next section discusses the extension of this technique to data collected with a three-channel phased array radar.

#### 2.3.3. Three Channel Signal Subspace Technique

The two-channel signal subspace method explained in Section 2.3.2 is extended for use with all three channels of the phased array radar depicted in Fig. 3. Once again, the lead channel will be channel 1 and the trailing channels will be 2 and 3. The Multi-channel Signal Subspace (MSS) extension to three channels will first project the range-Doppler image formed from the aligned motion compensated data of channel 2, $f_2(x,y)$, on to the basis functions defined by the range-Doppler image formed from the motion compensated data of channel 1, $f_1(x,y)$, and determine the spatially varying difference, $\hat{f}_{d2}(x_i,y_i)$, given by Equation 3. The resulting range-Doppler difference image of channels 1 and 2 is treated as a *new* independent channel, $f_4(x,y)$, as shown by

$$f_4(x,y) = \hat{f}_{d2}(x,y) = f_2(x,y) - \hat{f}_2(x,y). \quad (4)$$

Then the range-Doppler image formed by the aligned motion compensated data of channel 3, $f_3(x,y)$, is projected on to the basis functions defined by the range-Doppler image formed from the motion compensated data of channel 2, $f_2(x,y)$. The spatially varying difference, $\hat{f}_{d3}(x_i,y_i)$, from (3) is then determined. The resulting range-Doppler difference image of channels 2 and 3 in $f_5(x,y) = \hat{f}_{d3}(x,y) = f_3(x,y) - \hat{f}_3(x,y)$ is treated as a second *new* independent channel, $f_5(x,y)$, at a slightly different look angle.

Now the second *new* independent channel, $f_5(x,y)$, is projected on to the orthogonal basis functions of the first *new* independent channel, $f_4(x,y)$, represented by $\hat{f}_5(x,y) = f_4(x,y) \otimes \hat{h}_{45}(x,y)$.

The three-channel spatially-invariant difference image is represented as $\hat{f}_d(x,y) = f_5(x,y) - \hat{f}_5(x,y)$. The block processing represented by Equation 3 was applied to account for the spatially varying nature of the range-Doppler images.

Since each of the *new* independent channels is essentially a clutter-canceled range-Doppler image, this technique represents the fusion of two dual-channel clutter-suppressed range-Doppler images. The resulting *clutter-suppressed* range-Doppler image should contain more target features from the slightly different viewing antenna geometries in the array. The MSS method improves target features without enhancing any residual clutter in the *new* input images. Examples of this processing are presented in the section that follows.

### 2.4. Clutter-Suppression Results

The clutter-suppressed range-Doppler chips presented in this section were generated from the same part of the collected data discussed in Section 2.1. The moving target, a sedan, is slowing down while heading south, away from the radars' location. All of the range-Doppler chips presented in this section have a dynamic range of 50 dB with Doppler increasing from the left of the image to the right, and range increasing from the bottom of the image to the top. The DPCA algorithm result is presented first, then the two-channel MSS processed chips, and finally the three-channel clutter-suppressed result. The signal-to-noise ratio for all of the clutter-suppressed range-Doppler chips is computed for algorithm performance comparison.

The implementation of the DPCA algorithm required the first channel to be the lead channel and limited the amount of shifting that may occur to align the two channels. Therefore, only channels 1 and 2 could be processed to yield a clutter-cancelled range-Doppler image. The result is shown in Fig. 7. As stated earlier, the dynamic range is constant for all the results present in this section. However, adjusting the dynamic range of the DPCA range-Doppler chip would help better define the target.

Although the DPCA method could only produce clutter-cancelled chips from two of the three channels available, the multi-channel signal subspace (MSS) technique utilized all three channels in the processing. Fig. 8 is the clutter-suppressed range-Doppler image produced from channels 1 and 2. In comparing Fig. 8 to Fig. 7, the MSS approach does a better job of clutter cancellation than the baseline technique using the same data channels.

In Fig. 9, the clutter cancelled result of the MSS algorithm using channels 2 and 3 is presented. The relative reduction of clutter is similar to that of Fig. 8.

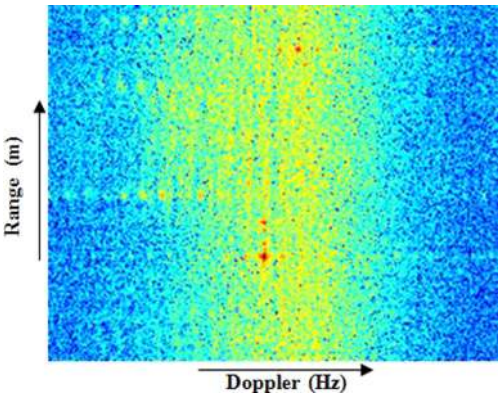


Fig. 7. DPCA clutter suppression technique.

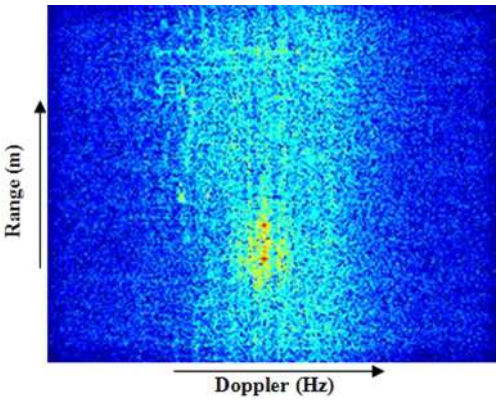


Fig. 8. MSS Two-channel clutter suppression technique: channels 1 and 2.

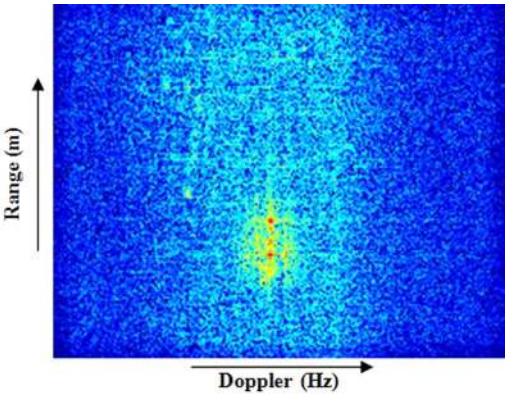


Fig. 9. MSS Two-channel clutter suppression technique: channels 2 and 3.

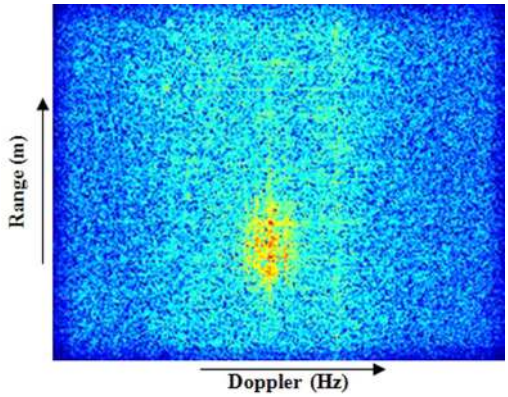


Fig. 10. MSS Three-channel clutter suppression technique.

Close examination of Figs. 8 and 9 reveal scattering from different locations of the target as well as more features in the range-Doppler imagery. This is caused in part by minor variations in the collection geometry due to the spacing of the antennas in the phased array radar.

Found in Fig. 10 is the clutter suppressed range-Doppler chip produced by the enhanced MSS algorithm using all three channels of the motion compensated data. A minor reduction in the level of clutter cancellation can be seen when comparing the results of Fig. 10 to that of Figs. 8 and 9. However, careful examination of the range-Doppler image in Fig. 10 shows more target features are present. The three-channel clutter suppressed image has a signal to noise level comparable to that of the MSS two-channel clutter-cancelled results and is an improvement over the baseline technique.

Finally, a signal-to-clutter ratio was determined for the chips presented in this section to help gauge the relative performance levels of the various techniques. This ratio was determined by finding the largest pixel value in the image; which is the brightest point on the target and dividing it by the average clutter in a one pixel wide frame around the entire range-Doppler chip. A comparison of the signal-to-clutter levels for the range-Doppler images formed from the three techniques discussed in this paper can be found in Table I.

TABLE I
DPCA vs. MSS Target to Clutter Ratio Comparison

| | |
|---|---|
| DPCA processing | 33.20 dB |
| MSS: 2 channel SS: channels 1 and 2 | 42.81 dB |
| MSS: 2 channel SS: channels 2 and 3 | 42.99 dB |
| MSS: 3 channel SS | 42.57 dB |

The MSS performance scales based on the comparable target-to-clutter ratios for both the two-channel and three-channel processing, with the three-channel MSS method resulting in a slightly noisier clutter-suppressed image, but with the added benefit of more target features being preserved after clutter cancellation. The results in Table I indicate that the MSS technique for traditional two-channel clutter cancellation and for multi-channel clutter suppression performs much better, nearly 10 dB in target to clutter ratio, than the DPCA method.

## 3. TARGET IDENTIFICATION FUSION

The ability to perform track and identity fusion requires sensor-processed classifications/identifications from different levels. Multi-target data association algorithms that accurately track targets in the presence of clutter assume that the detected targets can be tracked from a sequence of center-of-gravity and pose positional data. Detected classification can effectively discern the

target for a given scenario using experience of target movement, training, or predicted information. For example, two targets of the same type may be crossing in space, but since they can not occupy the same location, they would each have a different orientation relative to a sensor. By exploiting the orientation, velocity, and multi-resolution feature information, each target can be assessed for the correct track-ID association.

The capability of a sensor to track and identify targets simultaneously requires the target center, the target pose, and neighboring characteristics to discern salient features for target type association. For example, features [59] can be used to identify targets with a level of uncertainty. However, if many features are fused, the identity improves and helps eliminate clutter. The tracker must use the available features to discern an object (*identify* a target), which is a subset of Automatic Target Recognition (ATR). Certain features are inherently more useful in recognizing a target than others, but obtaining these features is a function of sensor resolution and collection geometry.

The 1-D HRR ATR known as the Baseline Automated Recognition of Targets (BART) algorithm has been used to generate identification results [22, 27]. BART is a template matching algorithm using the dominant range-space eigenvector. Eigen-templates have been used for 2D ATR problems using electro-optical [43], SAR, [42, 43], and Forward-Looking IR (FLIR) analysis [14, 15]. In each of these methods, the eigen-template matching provides a stable analysis for a single look. The eigenvector approach was then adapted and refined by Shaw [4, 52, 45] and others [18] for 1-D template formation using HRR profile data.

By leveraging knowledge about target features, fusion algorithms can significantly reduce processing time for tracking and identifying targets. For separated targets, resources may exist to identify each target. However, when resources and processing time are limited, a trade-off exists between the identification and tracking of a target. In the case of multiple ATR systems observing the same area, the HRR profiles can be at significantly different sensor-to-target geometries. Different geometries result in different features for target classification. In such a case, a decision-level fusion approach is a good solution since the ATR decisions are fused and not the features of the target signatures. By leveraging knowledge about target types, fusion algorithms can significantly reduce processing time for tracking and identifying targets. Increased robustness is achieved with a multi-look approach utilizing the eigen-template feature analysis [22], summarized by a classifier confusion matrix, and combined for enhanced HRR target identification.

### 3.1. Decision Level Fusion (DLF) Method

The decisions from an ATR are often stored in a confusion matrix (CM), which is an estimate of likelihoods. For the single-look ATR performance, these estimates are treated as priors [61]. Decisions from multiple ATRs or from multiple looks from different geometric perspectives are fused using the Decision Level Fusion (DLF) technique presented. With respect to the DLF, the CMs represent the historical performances of the ATR system. Assume that we have two ATRs each described in a confusion matrix designated as $C^A$ and $C^B$. The elements of a confusion matrix are $c_{ij} = \Pr\{\text{ATR decides } o_j \text{ when } o_i \text{ is true}\}$, where $i$ is the true object class, $j$ is the assigned object class, and $i = 1,\ldots,N$ for $N$ true classes. The CM elements can be represented as probabilities as $c_{ij} = \Pr\{z = j \mid o_i\} = p\{z_j \mid o_i\}$. To determine an object declaration, we need to use Bayes' rule to obtain $p\{o_i \mid z_j\}$ which requires the class priors, $p\{o_i\}$. We denote the priors and likelihoods as column vectors[1]

$$p(\bar{o}) = \begin{bmatrix} p(o_1) \\ p(o_2) \\ \vdots \\ p(o_N) \end{bmatrix} \qquad p(zj \mid \bar{o}) = \begin{bmatrix} p(zj \mid o_1) \\ p(zj \mid o_2) \\ \vdots \\ p(zj \mid o_N) \end{bmatrix}. \tag{5}$$

For $M$ decisions, a confusion matrix would be of the form

$$C = \begin{bmatrix} p(z1 \mid o_1) & p(z2 \mid o_1) & \cdots & p(zM \mid o_1) \\ p(z1 \mid o_2) & p(z2 \mid o_2) & \cdots & p(zM \mid o_2) \\ \cdots & \cdots & \ddots & \cdots \\ p(z1 \mid o_N) & p(z2 \mid o_N) & \cdots & p(zM \mid o_N) \end{bmatrix}. \tag{6}$$

The joint likelihoods are similar column vectors, where we assume independence for two confusion matrices $A$ and $B$ (denoted here as superscripts),

$$p(z_j^A, z_k^B \mid \bar{o}) = \begin{bmatrix} p(z_j^A \mid o_1) \cdot p(z_k^B \mid o_1) \\ p(z_j^A \mid o_2) \cdot p(z_k^B \mid o_2) \\ \cdots \\ p(z_j^A \mid o_N) \cdot p(z_k^B \mid o_N) \end{bmatrix} \tag{7}$$

where $k$ is used to distinguish between the different assigned object classes between the two confusion matrices when the CMs are not symmetric.

Using the priors and the likelihoods, we can calculate *a posteriori* from Bayes' Rule

$$p(\bar{o} \mid z_j^A, z_k^B) = \frac{p(z_j^A, z_k^B \mid \bar{o}) p(\bar{o})}{\sum_{i=1}^{N} p(z_j^A, z_k^B \mid \bar{o}) p(\bar{o})}. \tag{8}$$

[1] Based on FITE Memo, 15 May 2006, from Tim Ross.

```
function [d, pObarZaZb] = fuseCMdecisions(za, zb, Obar)
        CA = getConfusionMatrix(1);
        CB = getConfusionMatrix(2);
        pZaObar = CA(:,za);
        pZbObar = CB(:,zb);
        pZaZbObar = pZaObar .* pZbObar;
        posteriorNum = pZaZbObar .* pObar;
        posteriorDen = sum(posteriorNum);
        pObarZaZb = posteriorNum / posteriorDen;
        [junk, d] = max(pObarZaZb);
        return
```

Fig. 11. Confusion matrix pseudo code.

Note that there are similar column matrices for the posteriors $p(\bar{o} \mid zj)$ and $p(\bar{o} \mid z_j^A, z_k^B)$. A decision is made using the maximum likelihood estimate

$$d_i = \arg\max_{j;k} p(o_i | z_j^A, z_k^B) \tag{9}$$

where the final decision of the true object class $i$ is determined from the largest value from the vector.

Note that the subscripts indicate the value of a variable and the superscripts indicate the ATR source. For example, $z^A = z_3$ indicates that source $A$ made a decision $z_3$; where source $A$ might be the first look of a HRR ATR and decision $z_3$ might be target type "sedan." The absence of a superscript implies an unspecified single source. We represent the particular states from each source with the subscripts $a$ and $b$ such as $z^A = z_a^A$ indicating that source $A$'s decision was $z_a$.

For the developments of the pseudo code, shown below in Fig. 11, we shorten the notation to $z^A = z_a$, while keeping track of the confusion matrix source $A$ or $B$.

### 3.2. Naïve Bayes DLF Pseudocode

Inputs to the fuser are the decisions of ATR $A$ and $B$, i.e., $z_a$ and $z_b$ respectively. The output of the fuser is the decision $d$ based on a maximum a posteriori probability (MAP) decision rule, where the posterior is $p(\bar{o} \mid za, zb)$. The fuser must know the prior probabilities $p(\bar{o})$ and the confusion matrices (one for each source).

Pseudo code for DFL is represented as:

- za = $z_a$ and zb = $z_b$ are the integer decisions between $1 \ldots M$ of sources $A$ and $B$, respectively
- pObar = $p(\bar{o})$ is a vector of priors, represented as either constants or input variable
- CA = $C^A$ and CB = $C^B$ are the confusion matrices derived from sources $A$ and $B$, respectively
- pZaObar = $p(z_a \mid \bar{o})$ and pZbObar = $p(z_b \mid \bar{o})$ are the likelihoods as extracted columns from the confusion matrices [pZaObar = CA(:, za); and pZbObar = CB(:, zb)]
- pZaZbMbar = $p(z_a, z_b \mid \bar{o})$ is the joint likelihood derived from the point-wise product of the source likelihoods (pZaZbObar = pZaObar.∗pZbObar);
- pObarZaZb = $p(\bar{o} \mid z_a, z_b) = (p(z_a, z_b \mid \bar{o})p(\bar{o}))/(\sum_{i=1}^{N} \cdot p(z_a, z_b \mid \bar{o})p(\bar{o}))$
  —the numerator is:
  posteriorNum = pZaZbObar.∗pObar;
  —the denominator is:
  posteriorDen = sum(posteriorNum);
  —pMbarZaZb = posteriorNum/posteriorDen;
- $d$ = max(pObarZaZb), which is the fused decision, $d_i \ni p(o_i \mid z_a, z_b) \geq p(o_i \mid z_a, z_b) \quad \forall i, j$ where $i, j \in 1, \ldots, N$.

The DLF function pseudo code is presented for verification.

### 3.3. Metric Presentation

We used the eigen-value HRR target identification approach as a baseline method [27]. The likelihood vectors were compiled into a confusion matrix (CM). Thus, each single look provided a full analysis of the classifier, presented as a CM, for all target comparisons. The likelihood vectors of the confusion matrix allowed for a more thorough analysis with such performance criteria as declaration, $P_D$, and false alarm, $P_{FA}$, probabilities. The confusion matrix lists a set of likelihood values with the real targets as the rows $\{T_1, \ldots, T_N\}$, and the testable hypothesis as the columns $\{T_1, \ldots, T_N, \text{other}\}$. For example, if the true target is $T_1$, the CM is

$$CM = \begin{array}{c} \\ T_1 \\ T_2 \\ \\ T_N \end{array} \begin{array}{c} \begin{array}{ccccc} T_1 & T_2 & & T_N & \text{Other} \end{array} \\ \begin{bmatrix} A & B & \cdots & B & O \\ E & D & \cdots & D & O \\ \vdots & \vdots & \vdots & \vdots & \vdots \\ E & D & \cdots & D & O \end{bmatrix} \end{array}. \tag{10}$$

Selecting the likelihood values in the CM, one can compare the performance metrics for different size CMs. From the CM and a defined target-to-confusion ratio as $m$ (as set by the operational ATR requirements), a set of metrics can be identified to support analysis including

$$P_{\text{Declaration}} = \frac{A}{A + B} \tag{11}$$

$$P_{\text{FalseAlarm}} = \frac{E}{E + D} \tag{12}$$

$$P_{\text{CorrectClassification}} = \frac{m \cdot PD}{(m \cdot P_D) + P_{FA}}. \tag{13}$$

Using Fig. 21 as an example, let $A$ be the fact that target 1 is choice (row) and that target 1 is declared (column) by the ATR to produce a normalized likelihood of 0.63. The rows are normalized to one but rounding errors lead to values close to but not exactly equal to 1. $B = 0.075 + 0.12 + 0.56 + 0.042 = 0.293$. $E = 0.039 + 0.047 + 0.081 + 0.12 + 0.21 = 0.497$. $O$ is the entire right column of $0.084 + 0.02 + 0.054 + 0.039 + 0.025 + 0.21 = 0.432$. Finally, $D$ is the remaining value $D = 4.146$. Using the results from Fig. 21, then $P_{\text{Dec}} = 0.63/[0.63 + 0.293] = 0.683$. $P_{FA} = 0.497/[0.497 + 4.146] = 0.107$. If we let $m = 1$, then $P_{CC} = 0.683/[0.683 + 0.107] = 0.865$. These metrics are important in the fact that the

system is not forced to make a target declaration (column other) as well as ability to discern whether there is enough evidence to declare a target in the library [50].

By choosing a different target truth (row) to selection (column) as defined by the diagonal, the process is repeated for each true target and the resulting metrics are summed and normalized for the number of targets. For example, the second true target is

$$CM = \begin{array}{c} \\ T_1 \\ T_2 \\ \vdots \\ T_N \end{array} \begin{array}{c} \begin{array}{cccccc} T_1 & T_2 & & \cdots & T_N & \text{Other} \end{array} \\ \begin{bmatrix} D & E & D & \cdots & D & O \\ B & A & B & \cdots & B & O \\ \vdots & \vdots & \vdots & \vdots & \vdots & \vdots \\ D & E & D & \cdots & D & O \end{bmatrix} \end{array}. \tag{14}$$

## 4. IDENTIFICATION PERFORMANCE

Identification (ID) performance varies over three operating conditions: environment, sensors, and targets. To demonstrate environment variations, we compare adjacent versus separated target IDs for moving targets in Sections 4.1 and 4.2. To highlight the variations in sensors, we acknowledge the variations between the sensor-processing methods (DCPA versus MSS) throughout Section 4. Finally, for target variation, we show the confusion matrices results for single-look and multi-look comparisons in Sections 4.3–4.5.

The results that follow are from collected HRR profiles from moving targets. Simultaneous target tracking and ID requires using HRR radar mode that supports feature analysis in-between point movements (Moving Target Indicator—MTI mode) and 2-D stationary images (Synthetic Aperture Radar—SAR mode). In addition to enhanced target ID through higher-diagonal CM results, the clutter-suppression results demonstrate improved target localization. HRR feature analysis begins with aligning the HRR profile. Higher signature matches presented in the CM cell's results are indicative of more feature matches (including the length of the HRR target profiles).

Single-look confusion matrices were produced for 1-D HRR profiles formed from DPCA and MSS clutter canceled target chips for ten ground vehicles traveling along the roads shown in Fig. 4. Obscuration from nearby vegetation along the streets impacted identification performance depending on collection geometry. The DLF technique was then applied to five DPCA and five MSS single-look confusion matrices each produced with a unique sample set. The results of these experiments are presented in the subsections that follow.

### 4.1. Adjacent Vehicles

A subset of the data was selected to address a common target tracking issue, vehicle adjacency, and to compare identification performance among the various types of clutter canceled data in benign conditions. Three cars moving south along the western road shown in Fig. 4 were chosen because the vehicles are in the open and not obscured by vegetation. A bend in the road required the vehicles to decelerate and cluster closer together (less than one car length apart) while making the turn. The vehicle data near the bend in the road was divided from the vehicle data of the cars traveling south toward the bend in the road, creating two data sets: adjacent and separated. Note that these results are for an aspect angle centered around 180 degrees or near the rear of the vehicles.

Confusion matrix results were produced for the closely associated vehicles near the turn in the road. As targets slowed approaching the turn, the data was treated as the adjacency data set. The lead target had the fewest samples, and the trailing target had the most samples since it was waiting for the other targets to make the turn. Using the ID counts for each sample, we turned them into the scores in the single-look CM. Identification performance for the first two vehicles to arrive at the bend in the road was consistently poorer than the trailing vehicle that was less obscured. Note that the data included in Section 4.1 was used later in the overall results.

The identification performance using data sets for all clutter suppression methods are found in Figs. 12–15.

### 4.2. Separated Vehicles

The data of the three vehicles separated while traveling in the open was used to produce a "best case" identification performance comparison of each clutter suppression method. The recognition results for separated targets are presented in Figs. 16–19. It is noted from the CM, that the ID performance of all vehicles increases from $\sim 0.5$ to $\sim 0.85$. The ID performance of separated targets can be used in target confirmation, track maintenance, as well as afford resources to be applied to other search areas to acquire targets. To compare separated versus adjacent methods using the clutter cancellation, we summarize the results from the CMs.

A mean identification performance was computed for each matrix by averaging the diagonal of the CMs and is presented in Fig. 20 for comparison of the relative identification performance gains achieved by the techniques used. The three-channel signal subspace showed the best overall performance, followed by two channel signal subspace clutter cancelation with the two-channel DPCA having the poorest performance of the techniques compared. As expected, a high level of target identification of separated vehicles in benign conditions was achieved for all techniques examined.

### 4.3. Single-Look Performance

The identification performance comparisons presented in Sections 4.3, 4.4, and 4.5 are between the best (three-Channel MSS) and worst (DPCA) performing techniques in Sections 4.1 and 4.2.

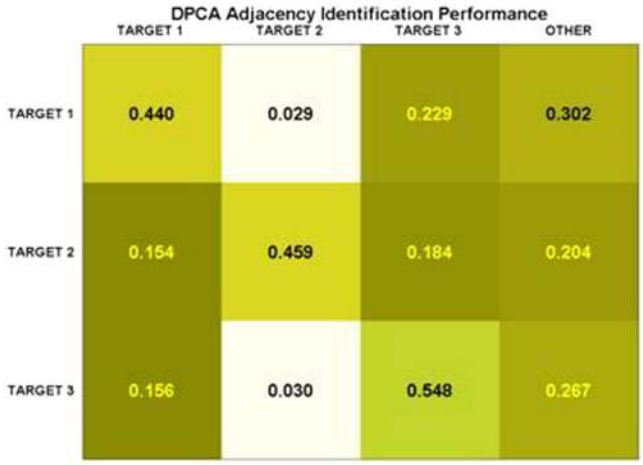


Fig. 12. DPCA single-look performance with target adjacency.

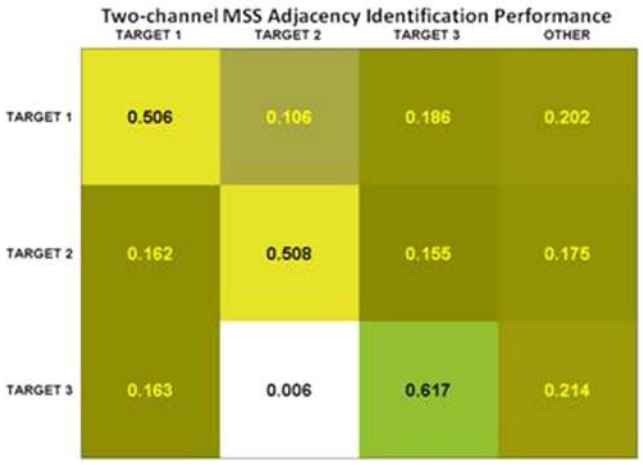


Fig. 13. Two-channel (1 and 2) MSS single-look performance with target adjacency.

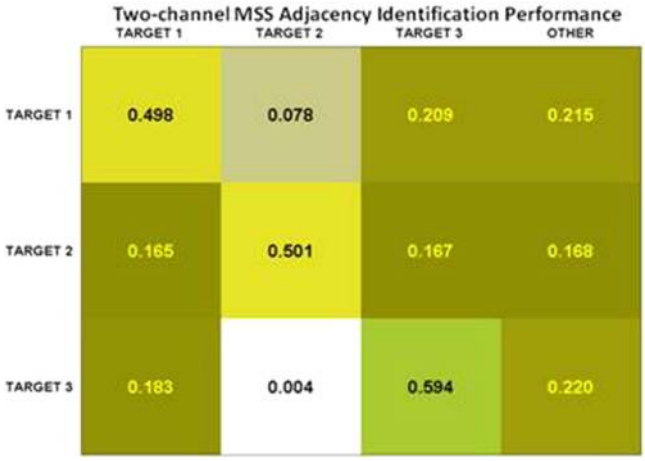


Fig. 14. Two-channel (2 and 3) MSS single-look performance with target adjacency.

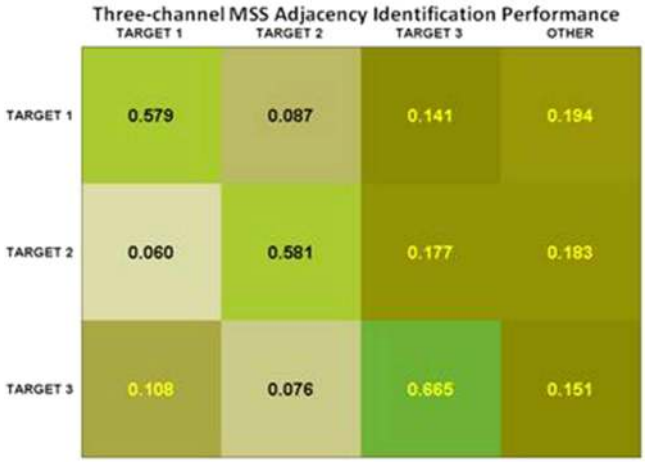


Fig. 15. Three-channel MSS single-look performance with target adjacency.

Five vehicles were selected for the library and the remaining five vehicles were used as confusers as was done in the companion papers [23, 24] for a total of ten templates. The libraries of target profiles were created from the off-line collected target signatures for this data set and compared to the on-line test data as used in [6]. To ensure 360 degree coverage, we used the entire data set to locate enough signatures to develop a 360 degree target signature database for training. After capturing the necessary training set, we used the remaining data for testing. For example, of the 1800 samples, we used about 1500 for training and the remaining 300 for testing.

The DPCA single-look identification results are shown in Fig. 21 with a mean target identification rate of 65%. The three-channel MSS single-look 1-D HRR ID performance is presented in Fig. 22 with an improved mean identification rate of 73.6% relative to the DPCA results.

The distribution of the confuser vehicles was spread across the not-in-library row for both the DPCA and MSS confusion matrices indicating no strong bias toward a library object.

A comparison of the receiver operator curve (ROC) associated with each of the HRR clutter cancelled data sets is presented in Fig. 23. The MSS clutter-suppressed data performs better with respect to the DPCA processed data.

### 4.4. Multi-look DLF Performance

Wider angle changes (different perspectives) would increase the ATR results. Instead of processing wider ($n$-channel) clutter suppression, we utilized Decision-Level Fusion (DLF) to incorporate angle changes for enhanced ATR results. The test data used for the DLF was the same as that used to create the single-look analysis. The DLF data included the entire scenario of the ten targets (five selected, five confusers) moving through different operating conditions of adjacency and separation, while the single-look analysis was a subset of only three targets in the specified operating condition over a shorter time interval.

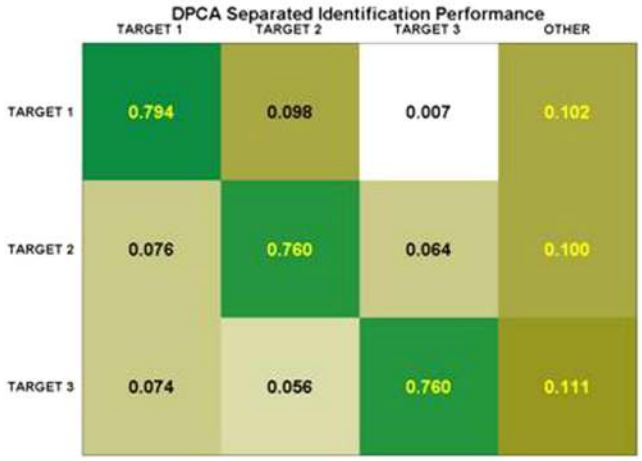


Fig. 16. DPCA single-look performance with separated targets.

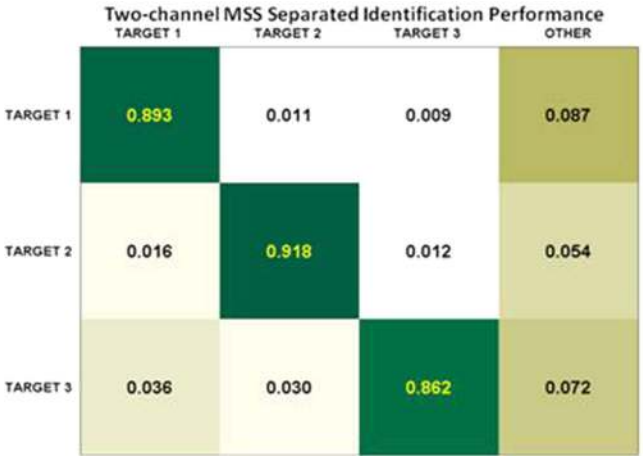


Fig. 17. Two-channel (1 and 2) MSS single-look performance with separated targets.

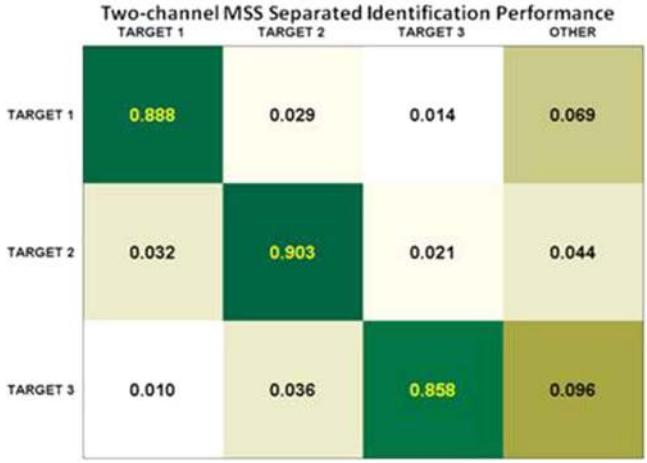


Fig. 18. Two-Channel (2 and 3) MSS single-look performance with separated targets.

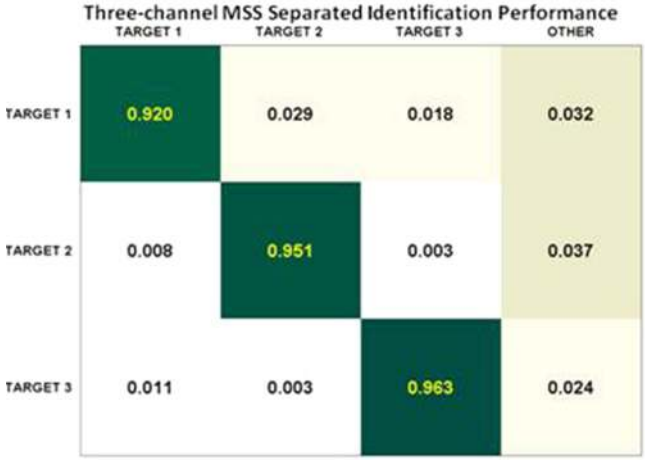


Fig. 19. Three-channel MSS single-look performance with separated targets.

The DLF algorithm described in Section 3.2 was run with confusion matrices 1 and 2 with the remaining confusion matrices being incorporated sequentially and the fused decision from the previous run being treated as prior knowledge of the targets of interest. This procedure was followed for both the DPCA and MSS single-look matrices. The fused DPCA target recognition results can be seen in Fig. 24 with significant performance gains relative to the single-look DPCA results of Fig. 21 and improved performance relative to the MSS single-look results of Fig. 22. Since the multi-look DPCA is better than the single-look MSS, there is value in utilizing multi-look DLF no matter which clutter suppression technique is used.

The best identification results for this scenario are shown in the MSS confusion matrix of Fig. 25 for multi-look DLF. The DLF off-diagonal target confusion was significantly reduced while correct ID was greatly enhanced relative to the DPCA processed data or single-look MSS target recognition. Average MSS DLF target ID increased to 89.2% for this moving target scenario relative to the single-look average DPCA vehicle recognition performance of 64.8%. Since the targets in the dynamic scenario are not always well separated, through DLF and three-channel MSS clutter suppression, the average target ID was better than the average DCPA best single look condition (Fig. 16) and equivalent to that of the average two-channel MSS best single look condition (Figs. 17 and 18).

A ROC comparison of the multi-look DLF performance is shown in Fig. 26. The Multi-channel Signal Subspace clutter suppressed data set has the best performance with respect to the fused DPCA data set and the single-look target identification results. The single-look performance of the MSS data set is comparable to the fused DPCA performance as illustrated by both the confusion matrices of Figs. 22 and 24 and the ROC curves found in Figs. 23 and 26. To further assess the similarities and differences in target identification performance relative to enhanced clutter suppression and fusion technique, the metrics of Section 3.2 are used on a per target basis and presented in the section that follows.

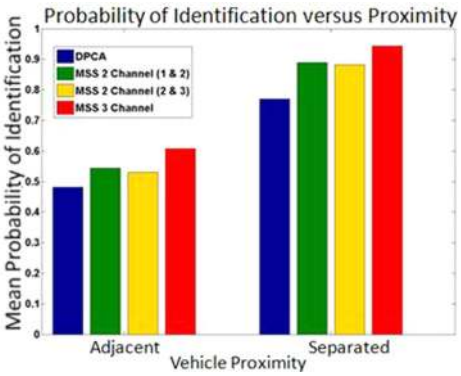


Fig. 20. Comparison of Mean Single-Look Identification Performance.

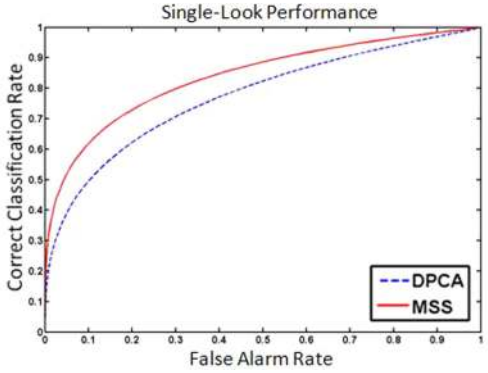


Fig. 23. Single-look ROC comparison.

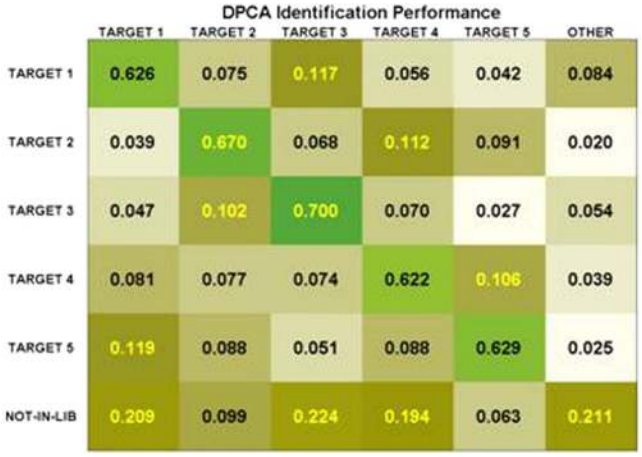


Fig. 21. DPCA single-look performance.

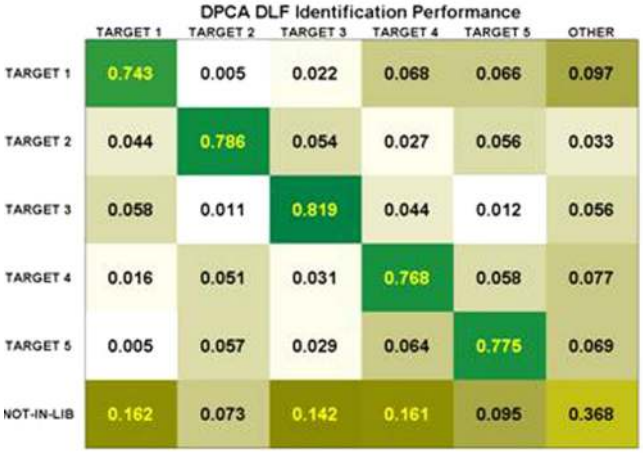


Fig. 24. DPCA decision-level fusion performance.

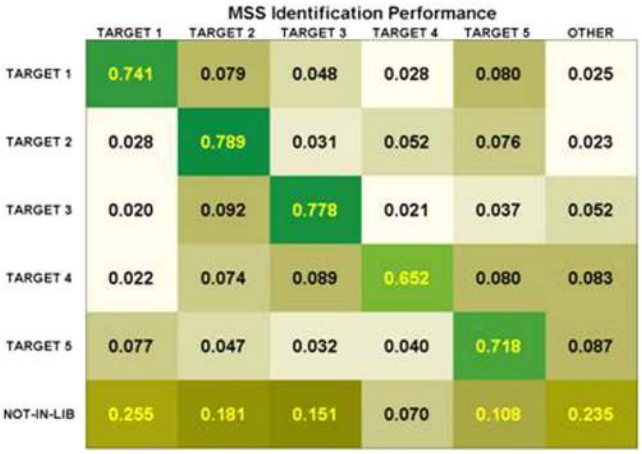


Fig. 22. Three-channel MSS single-look performance.

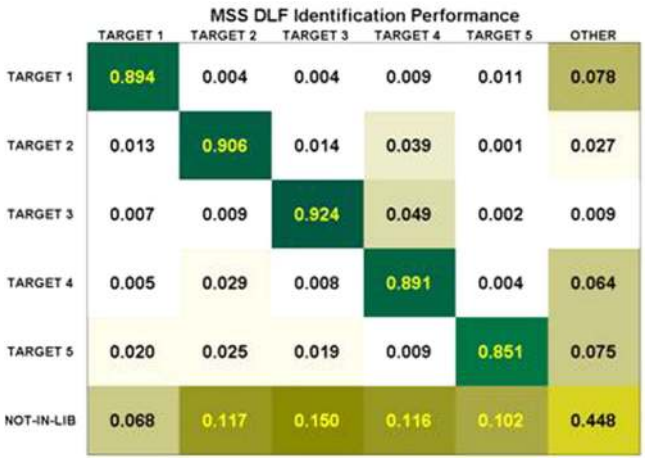


Fig. 25. Three-channel MSS decision-level fusion performance.

### 4.5. Performance Metrics

Fig. 27 shows the performance metrics computed using Equations 11–13 for each of the five in-library targets. Declaration, false alarm, and correct classification probabilities were compared for single-look DPCA (first blue bar), single-look MSS (second red bar), decision level fused multi-look DPCA (third yellow bar), and multi-look decision level fused MSS (fourth green bar) performance.

In general, target identification improves with enhanced clutter suppression and fused multi-look performance versus a single look ID. However, it is noted that not every example of MSS clutter cancellation results in improved individual target identification. An example of a false alarm increase was seen using the MSS in target 5. Using the DLF, both declaration and correct classification were improved. More importantly, with CM DLF, the false alarms were significantly reduced.

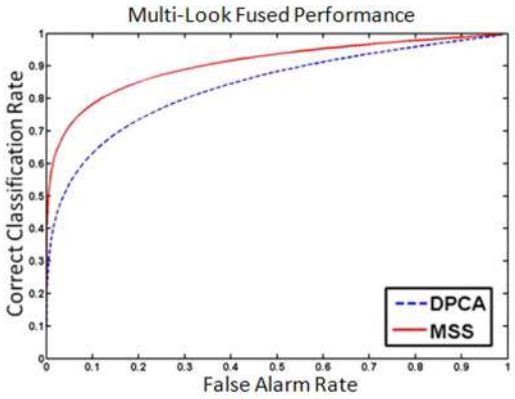


Fig. 26. Multi-look fusion ROC comparison.

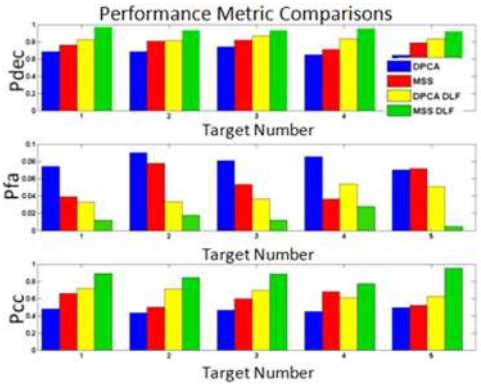


Fig. 27. DPCA and MSS single-look to multi-look performance metrics.

## 5. DISCUSSION AND CONCLUSIONS

The capability to collect and process three channels of radar data from a system configured with three phased-array antennas oriented in the along-track dimension has been demonstrated. The application of traditionally accepted two-channel clutter suppression techniques has been extended to true multi-channel data. The Multi-channel Signal Subspace (MSS) technique for two channels of data was demonstrated to be a superior clutter suppression technique to that of the Displaced Phase Center Antenna (DPCA) method. The MSS methodology was extended to exploit the additional information provided by the third channel of the phased array interrogating the scene.

The MSS technique applied to three channels of data suppressed the clutter well while preserving the features of the moving target. The signal-to-noise level of the three-channel MSS technique is approximately that of the two-channel MSS results. The availability of more target features in the range-Doppler image, while maintaining a good clutter suppression level, makes the MSS approach beneficial to automatic target recognition (ATR) applications. A significant ATR performance improvement is achieved with clutter suppressed data using the MSS algorithm relative to ATR performance with DPCA suppressed data.

A major factor not addressed in this paper; however, is that the processing time for the MSS algorithm is quite significant, especially when compared to the DPCA method. The processing times will need to be drastically reduced for the MSS algorithm to be practical in a data processing or operational environment. A potential solution is the parallelization of the time consuming block processing steps. This remains an area of future study.

The Confusion Matrix (CM) Decision-Level Fusion (DLF) multi-look technique improved target identification performance in comparison to the single-look ATR results. The CM-DLF algorithm performed extremely well with the MSS clutter suppressed data showing significant performance gains over both the single-look results and the DPCA fused performance. The DLF identification performance benefited from the target features preserved by the three-channel MSS clutter cancellation technique. For ATR applications, improved clutter suppression of HRR radar data greatly increases vehicle recognition and further enhances the resulting decision level fusion target identification of moving targets.

## ACKNOWLEDGMENTS

The authors would like to thank Tim Ross for significant discussions and coordination in the Confusion Matrix DLF development.

## REFERENCES

[1] D. Angelova and L. Mihaylova
Joint tracking and classification with particle filtering and mixture Kalman filtering using kinematic radar information.
*Digital Signal Processing*, **16**, 2 (Mar. 2006), 180–204.

[2] B. N. S. Babu, J. A. Torres, and W. L. Melvin
Processing and evaluation of multichannel airborne radar measurements (MCARM) measured data.
In *IEEE International Symposium on Phased Array Systems and Technology*, Oct. 1996.

[3] Y. Bar-Shalom and X-R. Li
*Multitarget-Multisensor Tracking: Principles and Techniques.*
YBS Publishing, Storrs, CT, 1995.

[4] V. Bhatnagar, A. K. Shaw, and R. W. Williams
Improved automatic target recognition using singular value decomposition.
In *Proceedings 1998 IEEE Conference on Acoustics, Speech, and Signal Processing*, vol. 5, 1998.

[5] S. Blackman and R. Popoli
*Design and Analysis of Modern Tracking Systems.*
Artech House, Boston, MA, 1999.

[6] E. Blasch
*Derivation of A Belief Filter for High Range Resolution Radar Simultaneous Target Tracking and Identification.*
Ph.D. Dissertation, Wright State University, 1999.

[7] E. Blasch
Assembling a distributed fused Information-based human-computer cognitive decision making tool.
*IEEE Aerospace and Electronic Systems Magazine*, **15**, 5 (May 2000), 11–17.

[8] E. Blasch and M. Bryant
Information assessment of SAR data for ATR.
In *Proceedings of IEEE National Aerospace and Electronics Conference*, 1998.

[9] E. Blasch and L. Hong
Data association through fusion of target track and identification sets.
In *International Conference on Information Fusion*, 2000.

[10] E. Blasch and S. Huang
Multilevel Feature-based fuzzy fusion for target recognition.
In *Proceedings of SPIE*, vol. 4051, 2000.

[11] E. Blasch, J. J. Westerkamp, J. R. Layne, L. Hong, F. D. Garber, and A. Shaw
Identifying moving HRR signatures with an ATR belief filter.
In *Proceedings of SPIE*, vol. 4053, 2000.

[12] E. Blasch and C. Yang
Ten methods to Fuse GMTI and HRRR measurements for joint tracking and identification.
In *International Conference on Information Fusion*, July 2004.

[13] L. E. Brennan and L. S. Reed
Theory of adaptive radar.
*IEEE Transactions on Aerospace and Electronic Systems*, **AES-9**, 2 (Mar. 1973), 237–252.

[14] L. A. Chan, N. M. Nasrabadi, and D. Torrieri
Discriminative eigen targets for automatic target recognition.
In *Proceedings of SPIE*, vol. 3371, 1998.

[15] L. A. Chan, N. M. Nasrabadi, and D. Torrieri
Eigenspace Transformation for automatic clutter rejection.
*Optical Engineering*, **40**, 4 (2001).

[16] H-C. Chiang, R. L. Moses, and L. C. Potter
Model based classification of radar images.
*IEEE Transactions on Information Theory*, **46**, 5 (Aug. 2000), 1842–1854.

[17] D. J. Choe and R. G. White
Moving target detection in SAR imagery: Experimental results.
In *IEEE International Radar Conference*, 1995, 644–649.

[18] F. Dicander and R. Jonsson
Comparison of Some HRR-classification algorithms.
In *Proceedings of SPIE*, vol. 4382, 2001.

[19] D. Gross, M. Oppenheimer, B. Kahler, B. Keaffaber, and R. Williams
Preliminary comparison of HRR signatures of moving and stationary ground vehicles.
In *Proceedings of SPIE*, vol. 4727, 2002.

[20] X. Guo and M. Soumekh
Signal subspace registration of time series medical imagery.
In *Proceedings of International Conference on Signal Processing*, 2002, 1524–1527.

[21] J. K. Jao
Theory of synthetic aperture radar imaging of a moving target.
*IEEE Transactions on Geoscience and Remote Sensing*, **39**, 9 (Sept. 2001), 1984–1992.

[22] B. Kahler and E. Blasch
Robust multi-look HRR ATR investigation through decision-level fusion evaluation.
In *International Conference on Information Fusion*, 2008.

[23] B. Kahler and E. Blasch
Impact of HRR radar processing on moving target identification performance.
In *International Conference on Information Fusion*, 2009.

[24] B. Kahler and E. Blasch
Target identification performance improvement from enhanced HRR radar clutter suppression.
In *Proceedings of the IEEE National Aerospace and Electronics Conference*, 2009.

[25] B. Kahler, E. Blasch, and L. Goodwon
Operating condition modeling for ATR fusion assessment.
In *Proceedings of SPIE*, vol. 6571, 2007.

[26] B. Kahler and B. Keaffaber
An improved multi-channel clutter suppression algorithm.
In *Proceedings of SPIE*, vol. 6568, 2007.

[27] B. Kahler, J. Querns, and G. Arnold
An ATR challenge problem using HRR data.
In *Proceedings of SPIE*, vol. 6970, 2008.

[28] R. Klemm
Introduction to space-time adaptive processing.
*IEE ECEJ, special issue on STAP*, **11**, 1 (Feb. 1999), 5–12.

[29] R. Klemm
Prospectives in STAP research.
In *Proceedings of the 2000 IEEE Sensor Array and Multichannel Signal Processing Workshop*, Mar. 2000, 7–11.

[30] G. Krieger, N. Gebert, and A. Moreira
Unambiguous SAR signal reconstruction from non-uniform displaced phase center sampling.
*IEEE Geoscience and Remote Sensing Letters*, **1**, 4 (Oct. 2004), 260–264.

[31] B. V. Kumar and M. Alkanhal
Eigen-extended maximum average correlation height (EEMACH) filters for automatic target recognition.
In *Proceedings of SPIE*, vol. 4379, 2001.

[32] J. Lancaster and S. Blackman
Joint IMM/MHT tracking and identification for multisensor ground tracking.
In *International Conference on Information Fusion*, 2006.

[33] B. Liu
Clutter suppression using recursive and non-recursive MTI filters.
*IEEE Transactions on Aerospace and Electronic Systems*, **24**, 3 (May 1988), 210–217.

[34] R. A. Mitchell and J. J. Westerkamp
Robust statistical feature based aircraft identification.
*IEEE Transactions on Aerospace and Electronic Systems*, **35**, 3 (July 1999), 1077–1094.

[35] C. E. Muehe and M. Labitt
Displaced-phase-center antenna technique.
*Lincoln Laboratory Journal*, **12**, 2 (2000).

[36] S. Mori, C-Y. Chong, E. Tse, and E. P. Wishner
Tracking and classifying multiple targets without a priori identification.
*IEEE Transactions on Automatic Control*, **AC-31**, 5 (May 1986), 401–409.

[37] W. E. Ng, C. B. Zhang, Y. H. Lu, and T. S. Yeo
Simulated DPCA performance for dual-channel SAR processing.
In *IEEE International Geoscience and Remote Sensing Symposium*, 1999.

[38] S. G. Nikolov, E. Fernandez Canga, J. J. Lewis, A. Loza, D. R. Bull, and C. N. Canagarajah
Adaptive image fusion using wavelets: Algorithms and system design.
In E. Lefebvre and P. Valin (Eds.), *Multisensor Data and Information Processing for Rapid and Robust Situation and Threat Assessment*, IOS Press, 2006.

[39] T. Nohara
Derivation of a 3-channel DPCA/monopulse radar using phased arrays.
*IEEE National Telesystems Conference*, 1994, 243–246.

[40] T. Nohara
Comparison of DPCA and STAP for space-based radar.
In *IEEE International Radar Conference*, 1995, 113–119.

[41] T. Nohara, P. Scarlett, and B. Eatock
A radar signal processor for space-based radar.
In *IEEE National Radar Conference*, 1993.

[42] L. M. Novak and G. J. Owirka
Radar target identification using an eigen-image approach.
In *IEEE Radar Conference*, 1994.

[43] L. M. Novak, G. J. Owirka, and A. L. Weaver
Automatic target recognition using enhanced resolution SAR data.
*IEEE Transactions on Aerospace and Electronic Systems*, **35**, 1 (Jan. 1999), 157–175.

[44] K. Ohba and K. Ikeuchi
Recognition of multi-specularity objects using the eigen-window.
In *IEEE 1996 Proceedings of the 13th International Conference on Pattern Recognition*, 1996, 692–696.

[45] S. Paul and A. K. Shaw
Robust HRR radar target identification by hybridization of HMM and eigen-template-based matched filtering.
In *Proceedings of SPIE*, vol. 5094, 2003.

[46] S. Paul, A. K. Shaw, K. Das, and A. K. Mitra
Improved HRR-ATR using hybridization of HMM and eigen-template-matched filtering.
In *IEEE Conference on Acoustics, Speech, and Signal Processing*, 2003.

[47] K. Ranney and M. Soumekh
Signal subspace change detection in averaged multi-look SAR imagery.
In *Proceedings of SPIE*, vol. 5808, 2005.

[48] P. G. Richardson
Analysis of the adaptive space time processing technique for airborne radar.
*IEE Proceedings—Radar, Sonar Navigation*, **141**, 4 (Aug. 1994), 187–195.

[49] P. G. Richardson
Effects of manoeuvre on space time adaptive processing performance.
In *IEEE Radar 97 Conference*, Pub. No. 449, Oct. 1997, 285–289.

[50] T. D. Ross, W. E. Pierson, E. G. Zelnio, and K. L. Priddy
Detection system performance metrics with scene content dependencies.
In *Proceedings of SPIE*, vol. 5808, 2005.

[51] K. Shaw and V. Bhatnagar
Automatic target recognition using eigen-templates.
In *Proceedings of SPIE*, vol. 3370, 1998.

[52] K. Shaw, R. Vashist, and R. Williams
HRR-ATR using eigen-template with noisy observations in unknown target scenario.
In *Proceedings of SPIE*, vol. 4053, 2000.

[53] W. Snyder, G. Ettinger, and S. Laprise
Modeling performance and image collection utility for multiple look ATR.
In *Proceedings of SPIE*, vol. 5427, 2004.

[54] M. Soumekh
Signal subspace fusion of uncalibrated sensors with application in SAR, diagnostic medicine and video processing.
*IEEE Transactions on Image Processing*, **8**, 1 (Jan. 1999), 127–137.

[55] M. Soumekh
*Synthetic Aperture Radar with MATLAB Algorithms*.
New York, NY: John Wiley & Sons, Inc., 1999.

[56] M. Soumekh
Moving target detection and imaging using an X band along-track monopulse SAR.
*IEEE Transactions on Aerospace and Electronic Systems*, **38**, 1 (Jan. 2002), 315–333.

[57] M. Soumekh and B. Himed
SAR-MTI processing of multi-channel airborne radar measurement (MCARM) data.
In *Proceedings of IEEE Radar Conference*, 2002.

[58] M. Soumekh, S. Worrell, E. Zelnio, and B. Keaffaber
SAR wavefront reconstruction using motion compensated phase history (polar format) data and DPCA-based GMTI.
In *Proceedings of SPIE*, vol. 4053, 2000.

[59] W. Streilein, A. Waxman, W. Ross, F. Liu, M. Braun, D. Fay, P. Harmon, and C. H. Read
Fused multi-sensor image mining for feature foundation data.
In *International Conference on Information Fusion*, 2000.

[60] A. Tchamova, J. Dezert, T. Semerdjiev, and P. Konstantinova
Target tracking with generalized data association based on the general DSm rule of combination.
In *International Conference on Information Fusion*, 2004.

[61] J. D. Thompson
Verification of a decision level fusion algorithm using a proven ATR system and measured SAR data.
M.S. Thesis, Air Force Institute of Technology, 2006.

[62] R. Williams, J. Westerkamp, D. Gross, and A. Palomino
Automatic target recognition of time critical moving targets using 1D high range resolution (HRR) radar.
*IEEE Aerospace and Electronic Systems Magazine*, **15**, 4 (Apr. 2000), 37–43.

[63] R. Wu, Q. Gao, J. Liu, and H. Gu
ATR scheme based On 1-D HRR profiles.
*Electronic Letters*, **38**, 24 (Nov. 2002), 1586–1588.

[64] C. Yang and E Blasch
Mutual aided target tracking and identification.
*Proceedings of SPIE*, vol. 5099, 2003.

[65] C. Yang and E. Blasch
Pose angular-aiding for maneuvering target tracking.
*International Conference on Information Fusion*, 2005.

[66] C. Yang and E. Blasch
Pose-angular tracking of maneuvering targets with high range resolution radar (HRR).
*International Conference on Information Fusion*, 2008.

[67] C. Yang, E. Blasch, W. Garber, and R. Mitchell
A net track solution to pose-angular tracking of maneuvering targets in clutter with HRR radar.
*IEEE Conference on Signals, Systems and Computers*, 2007.